LANGMUIR

pubs.acs.org/Langmuir Article

Assessing the Structure and Equilibrium Conditions of Complex Coacervate Core Micelles by Varying Their Shell Composition and Medium Ionic Strength

Júlia Bonesso Sabadini, Cristiano Luis Pinto Oliveira, and Watson Loh*

Cite This: *Langmuir* 2024, 40, 2015−2027 Read Online

ACCESS | Metrics & More | Article Recommendations | Supporting Information

ABSTRACT: Complex coacervates result from an associative phase separation commonly involving oppositely charged polyelectrolytes. When this associative interaction occurs between charged-neutral diblock copolymers and oppositely charged homopolymers, a nanometric aggregate called a complex coacervate core micelle, C3M, is formed. Recent studies have addressed the issue of their thermodynamic or kinetic stability but without a clear consensus. To further investigate this issue, we have studied C3Ms formed by the combination of poly(diallyldimethylammonium) and copolymer poly(acrylamide)-*b*-poly(acrylate) using different preparation protocols. Dynamic light scattering and small-angle X-ray scattering measurements suggest that these structures are in an equilibrium condition because the aggregates do not vary with different preparation protocols or upon aging. In addition, their stability and structures are critically dependent on several parameters such as the density of neutral blocks in their shell and the ionic strength of the medium. Decreasing the amount of copolymer in the system and, hence, the density of neutral blocks in the shell results in an increase in the aggregate size because of the core growth, although their globular shape is retained. On the other hand, larger clusters of micelles were formed at higher ionic strengths. Partially replacing 77% of the copolymer with a homopolymer of the same charge or increasing the ionic strength of the system (above 100 mmol L^{-1} NaCl) leads to a metastable state, after which phase separation is eventually observed. SAXS analyses reveal that this phase separation above a certain salt concentration occurs due to the coagulation of individual micelles that seem to retain their individual globular structures. Overall, these results confirm earlier claims that equilibrium C3Ms are achieved close to 1:1 charge stoichiometry but also reveal that these conditions may vary at different shell densities or higher ionic strengths, which constitute vital information for envisioning future applications of C3Ms.

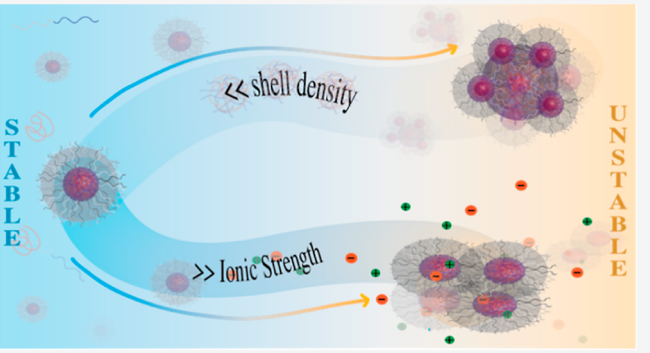

INTRODUCTION

Complex coacervation refers to an associative liquid−liquid phase separation commonly involving oppositely charged polyelectrolytes in an aqueous solution, with the resultant coacervate concentrated in one of the phases.[1] Concerning the thermodynamic aspects of coacervation, it has been shown that entropy is the main driving force and that increase is caused by the release of counterions and water molecules solvating the polyelectrolytes.[2,3] Calorimetric experiments revealed that the complexation can be either exothermic or endothermic, depending, for example, on salt concentration.[4] Therefore, the spontaneity for complex coacervation is highly sensitive to the type and concentration of the ions present, with the complex only formed below a critical ionic strength. This is expected considering that the driving force decreases upon increasing the ionic strength as the concentration of ions in the double layer of the polyelectrolytes and the bulk solution tend toward equality.[5]

Coacervates can be constrained to colloidal dimensions, provided that one of the polyelectrolytes is replaced by a charged-neutral diblock copolymer. These aggregates are called complex coacervate core micelles (or C3Ms). They consist of a core, comprising the associative complex, and a shell formed by the hydrophilic part of the copolymer, thus resembling surfactant micelles.[6] Recent studies have demonstrated that C3Ms are promising structures for a variety of applications, such as in catalysis,[7−9] as sensors,[10] for encapsulation,[11−13] and controlled delivery,[14,15] which are relevant properties to be explored, especially in the biomedical field.[16,17] Two aspects are crucial to understand when designing C3Ms for specific

Received: June 13, 2023
Revised: January 3, 2024
Accepted: January 4, 2024
Published: January 19, 2024

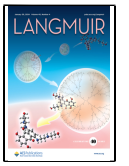

https://doi.org/10.1021/acs.langmuir.3c01606
Langmuir 2024, 40, 2015−2027

purposes: their mechanism of formation and the stability of the aggregates. The definition of the limits for the thermodynamic and kinetic stability of C3Ms is a key point, intensively discussed in the literature.[18−23]

Hofs et al.[23] demonstrated the importance of the charge equivalence between polyions for the formation of dense micelles. According to those authors, there is a concentration range of positive and negative charges of the polyelectrolytes, close to 1:1, which is favorable to the formation of the thermodynamically stable C3M. Such a condition was called the preferred micellar composition (PMC), and far from the PMC, the excess of charge hinders the aggregation into micellar objects. This happens because although the interaction between the polyelectrolytes occurs, the formation of larger and dense aggregates is unfavorable due to the excess of charges being confined in the core.

Burgh and co-workers have proposed a thermodynamic model to account for the stability of C3Ms.[18] According to this model, some aspects are important for providing stability conditions, such as the block length of the diblock copolymers and the molecular weight of the homopolymer. They also emphasized that the stability and aggregation mechanism depend on the nature of the ionic groups of the polyelectrolytes as well as on the chemical nature of the neutral corona (shell). Those authors postulated that the free energy for the formation of micelles, $F_{micelle}$, may be divided into several contributions, as follows

$$F_{micelle} = F_{surface} + F_{shell} + F_{core} + F_{complex} \quad (1)$$

The subscripts in eq 1 refer, respectively, to contributions from the free energy of the interface, the shell, the core, and the complex, the last one being the unique term that contributes favorably to the stabilization of the aggregates. Like coacervate formation, for C3M, the process is driven mainly by the same entropic contributions. However, for C3M formation, other terms need to be considered. They are related to the entropic penalty associated with the stretching of the macromolecules in the core and shell, which are included in the $F_{core,}$ and F_{shell}, respectively. Finally, the term $F_{surface}$ is due to the creation of a contact area between the solvent and coacervate cores. According to this approach, another prerequisite for C3M stability is associated with the ratio between neutral and charged parts of the block copolymer. For instance, for a copolymer with very asymmetric blocks, the formation of stable micelles would not be favored.

The formation of C3Ms is usually affected by some effects such as conformation restrictions, lack of charge complementarity, and competition between repulsion and attraction.[19−21] Despite all those aspects that can result in kinetically trapped nonequilibrium states,[19,20] C3M structures are reported to follow relaxation[11] and relatively fast exchange. Holappa et al.[24] experimentally studied the dynamic processes involving C3Ms. According to them, fast and slow events are involved in C3M formation. The fast one (within the range of seconds) is associated with the exchange of diblock copolymer chains between two aggregates by the expulsion/reinsertion mechanism. The slow one (within the time scale of minutes) corresponds to the merging and splitting of two micelles. Bakeev et al.[25] stressed that the ionic strength and the charge ratio between the polyelectrolytes greatly influence micellar dynamics. They concluded that by increasing salt concentration, these events become faster.

Furthermore, Wu et al.[19] studied the importance of the preparation pathways on the properties of these electrostatic complexes, revealing that their thermodynamic or kinetic control could be discriminated. For this purpose, two preparation routes were used. In one, salt was added previously to the isolated polyelectrolytes and, in the other, the addition was carried out in the system with the complex already formed. They concluded that a stable product was obtained via the first route but that the second procedure led to a metastable structure. Recently, Kim et al.[26] also verified a pathway dependence for the formation of C3Ms. They observed that heterogeneous and large C3Ms were obtained when the aggregates were prepared by simply mixing. The addition of a simple salt resulted in the collapse of those structures. However, C3Ms were restored upon ion removal by dialysis.

As we described above, C3M stability is still elusive, and this prompted the present study in which we assess the stability of C3Ms formed by a charged-neutral diblock copolymer, poly(acrylamide)-*b*-poly(acrylic acid) (PAAm-*b*-PAA), and an oppositely charged homopolymer, poly(diallyldimethylammonium chloride) (PDADMAC). The effects of changes in C3M composition, of replacing block copolymer with homopolymer and hence decreasing the content of neutral blocks in their shell, and of varying ionic strength on the C3Ms' structure and stability were investigated over time by dynamic light scattering (DLS) and small-angle X-ray scattering measurements. To eliminate all simple salt contributions, C3Ms were prepared using a methodology based on an acid−base titration, leading to the so-called complex salts.[27,28] Based on these results, the boundaries of thermodynamic and kinetic regimes were assessed in an attempt to shed more light on the fundamental aspects of these important self-assembly structures.

MATERIALS AND METHODS

Materials. The poly(acrylamide)-*b*-poly(acrylic acid) diblock copolymers, abbreviated as $PAAm_{25}$-*b*-PAA_{65} and $PAAm_{95}$-*b*-PAA_{65}, were synthesized and characterized as described previously.[29] The subscripts refer to the weight-average number of repeat units of each block. These polymers were characterized by proton nuclear magnetic resonance (^{1}H NMR) and gel permeation chromatography (GPC), and their features are summarized in Table 1.

Table 1. Weight Average Molar Mass of the Copolymer Blocks and Dispersity ($Đ$) of PAAm-*b*-PAA

block copolymer	PAAm/g mol^{-1}	PAA/g mol^{-1}	$Đ^a$
$PAAm_{25}$-*b*-PAA_{65}	1895	4508	2.3
$PAAm_{95}$-*b*-PAA_{65}	6773	4508	3.5

$^a Đ = M_w/M_n$, as determined by gel permeation chromatography.

Solutions of cationic homopolymer, poly(diallyldimethylammonium chloride), with two different average molar masses, M_w < 100,000 g mol^{-1} (referred to as $PDADMAC_S$) and 100,000 < M_w < 200,000 g mol^{-1} (referred to as $PDADMAC_L$), with concentrations of 25 and 35% wt, respectively, were purchased from Sigma-Aldrich (USA). Their actual concentrations were determined to be 2.1 × 10^{-3} mol of monomers g^{-1} and 1.3 × 10^{-3} mol of monomers g^{-1} via potentiometric titration, using an Ag/AgCl electrode. Poly(acrylic acid) homopolymer with a molar mass of 2000 g mol^{-1} (PAA_{30}), the anion-exchange resin Dowex Monosphere 550A (OH), sodium chloride, and sodium hydroxide were also procured from Sigma-Aldrich (USA).

Preparation of Polyelectrolyte Complex Containing Their Small Counterions (Referred to as Direct Mixing Method-

https://doi.org/10.1021/acs.langmuir.3c01606
Langmuir 2024, 40, 2015−2027

ology). Individual dilute aqueous solutions containing copolymer $PAAm_{95}$-*b*-PAA_{65} and homopolymers of $PDADMAC_S$ with the same charge concentration were prepared. These solutions were mixed, and then, the pH was adjusted to 7.5 ± 0.3 using NaOH solution in order to have the same final pH obtained when the complex salt was dissolved (in the concentration of 0.015% wt). The solutions were also filtered through a 220 nm polyvinylidene fluoride (PVDF) filter before use.

Preparation of Polyelectrolyte Complex Free of Small Ions—Complex Salts (Referred to as Acid−Base Titration Methodology). This preparation methodology was proposed to produce polyelectrolyte complexes in the absence of their small counterions.[29−31] Briefly, a 2% wt PDADMAC solution is submitted to an ion exchange process using a hydroxide-treated resin. The resulting hydroxide form, PDADMAOH, was then immediately titrated with a 0.1 mol L^{-1} PAAm-*b*-PAA solution (based on acrylate monomers) until the equivalence point, usually at pH 8.8−9.3. The final system was freeze-dried to produce powders, which were kept in a desiccator. The resulting product with a 1:1 charge stoichiometry is free of counterions and is referred to as a complex salt. Since the complex salts are formed by the interaction between the anionic poly(acrylate) (PA) and the catanionic poly-(diallyldimethylammonium) (PDADMA), it will be represented as $PAAm_{25}$-*b*-($PA_{65}PDADMA_S$), $PAAm_{25}$-*b*-($PA_{65}PDADMA_L$), $PAAm_{95}$-*b*-($PA_{65}PDADMA_S$), and $PAAm_{95}$-*b*-($PA_{65}PDADMA_L$) according to the block length of the copolymers and the homopolymer length. Complex salt aqueous solutions were obtained by dissolving the complex powder in water at the desired concentration (reaching a final pH of 7.5 ± 0.3 in 0.015% wt). The solutions were filtered through a 220 nm poly(vinylidene fluoride) (PVDF) filter before use.

Preparation of Complex with Partial Replacement of the Charged-Neutral Diblock Copolymer (Shell Composition). This procedure aims to prepare C3M by varying its shell composition. For that, a similar acid−base titration methodology was employed to prepare a polyelectrolyte complex with an overall 1:1 charge stoichiometry but with the partial replacement of the copolymer, $PAAm_{95}$-*b*-PAA_{65}, by the homopolymer, PAA_{30}. The hydroxide form of the polycation (PDADMAOH) was titrated with an aqueous solution containing both $PAAm_{95}$-*b*-PAA_{65} and PAA_{30} at the desired ratio until the equivalence point (same pH range as before). Different ratios of block copolymer and anionic homopolymer were investigated: 50:50 and 23:77.

Samples with Simple Salt Addition. For these studies, a fixed amount of the freeze-dried solid complex $PAAm_{25}$-*b*-($PA_{65}PDADMA_S$) and $PAAm_{95}$-*b*-($PA_{65}PDADMA_S$) (prepared using the acid−base titration methodology) was solubilized in solutions of different NaCl concentrations in the range 1−300 mmol L^{-1} (the final polymer concentration was 0.015% wt).

TECHNIQUES

Zeta Potential Measurements. Electrophoretic mobility measurements were performed using Malvern NanoZS Zetasizer equipment with a 632.8 nm laser and the detector positioned at 173°. Samples were placed in folded capillary cuvettes and measured at 25.0 ± 0.1 °C in all experiments. The Smoluchowski model was used to calculate the zeta potential values (ζ) for the C3Ms.

DLS Experiments. Light scattering experiments were conducted in a CGS-3-based goniometer system, ALV-GmbH, Langen, Germany, equipped with a detection system in a pseudocross-geometry, with a 22 mW He−Ne laser (λ = 632.8 nm) and an ALV 7004 multitau correlator. *cis*-Decalin was used as the refractive index-matching liquid, and the temperature was controlled at 25 ± 0.1 °C. The samples were prepared by weighting the polyelectrolyte complexes and deionized water, and they were filtered through a 220 nm poly(vinylidene fluoride) (PVDF) filter directly into borosilicate glass cells. DLS measurements were performed at the detection angle (θ) range of 30−150° with an increment of 10° for 0.015% wt samples. The apparent diffusion coefficient, D_0, was obtained considering the expression $\Gamma(q) = D_0q^2$. Here, $\Gamma(q)$ denotes the correlation function decay rate at the scattering wave-vector, $q = \frac{4\pi n}{\lambda}\sin\frac{\theta}{2}$, where n is the refractive index and λ represents the laser wavelength. From values of D_0 and using the Stokes−Einstein approximation for translational diffusion, the hydrodynamic radius, R_H, was determined.

For experiments aiming at testing their time aging, effects of the simple salt, and partial replacement of the copolymer, the DLS measurements were carried out at 90° for 0.015% wt samples. The hydrodynamic radius and relaxation time distribution were determined by using the CONTIN analyses of the autocorrelation function and the Stokes−Einstein approximation. These measurements were carried out in duplicate. The polydispersity of the size distribution of the aggregates could also be analyzed based on the polydispersity index (PDI). This parameter for an individual size distribution is the square of the standard deviation divided by the square of the average size.

Small Angle X-ray Scattering Experiments. The small angle X-ray scattering (SAXS) technique was used to investigate the size and shape of C3Ms in different conditions. SAXS experiments were performed using the laboratory-based system Xeuss 2.0 (Xenocs) at the Institute of Physics of the University of São Paulo. The equipment was used with a GeniX 3D X-ray source with a copper target (λ = 1.52) and a FOX3D collimation optic. The sample-to-detector distance used was 3.80 m, resulting in a q-range of 0.00275−0.10334 $Å^{-1}$. SAXS images were collected on a PILATUS 300k 2D photon counting detector. The samples were placed on homemade liquid sample holders composed of glass capillaries of 1.5 mm in diameter, glued to stainless steel cases. The holders are closed with caps containing rubber sealing. Therefore, it is possible to wash and rinse the sample holders and measure them under vacuum. The samples and buffers were measured in the same capillaries, maintained at a temperature of 25 °C. Azimuthal integration of the 2D scattering images was performed using the program package Fit2D[32]. The obtained 1D curves were subjected to standard data treatment procedures using the SUPERSAXS program package (Oliveira, C.L.P.; Pedersen, J.S., unpublished). This software also provides estimates for errors in scattering intensities. Absolute scale normalization was performed using the known absolute scattering intensity of water at a temperature of 20 °C.

The scattering intensity is displayed as a function of the scattering vector modulus, which is defined as $q = \frac{4\pi}{\lambda}\sin\frac{\theta}{2}$, where θ is the scattering angle and λ is the incident radiation wavelength. The obtained SAXS intensities can be written as the contribution of the normalized form factor $P(q)$, the structure factor $S(q)$, and the density of particles N/V

$$I(q) = \frac{N}{V}P(q)S(q) \tag{2}$$

The description of the form and structure factors depends on the investigated system. $P(q)$ is related to the particle sizes and shapes, and the $S(q)$ can provide indications on particle interactions and aggregation. For systems without clear structure factor effects, its value can be set to unity, and the scattering intensity will be proportional to the intensity scattered by a single particle.[33]

https://doi.org/10.1021/acs.langmuir.3c01606
Langmuir 2024, 40, 2015−2027

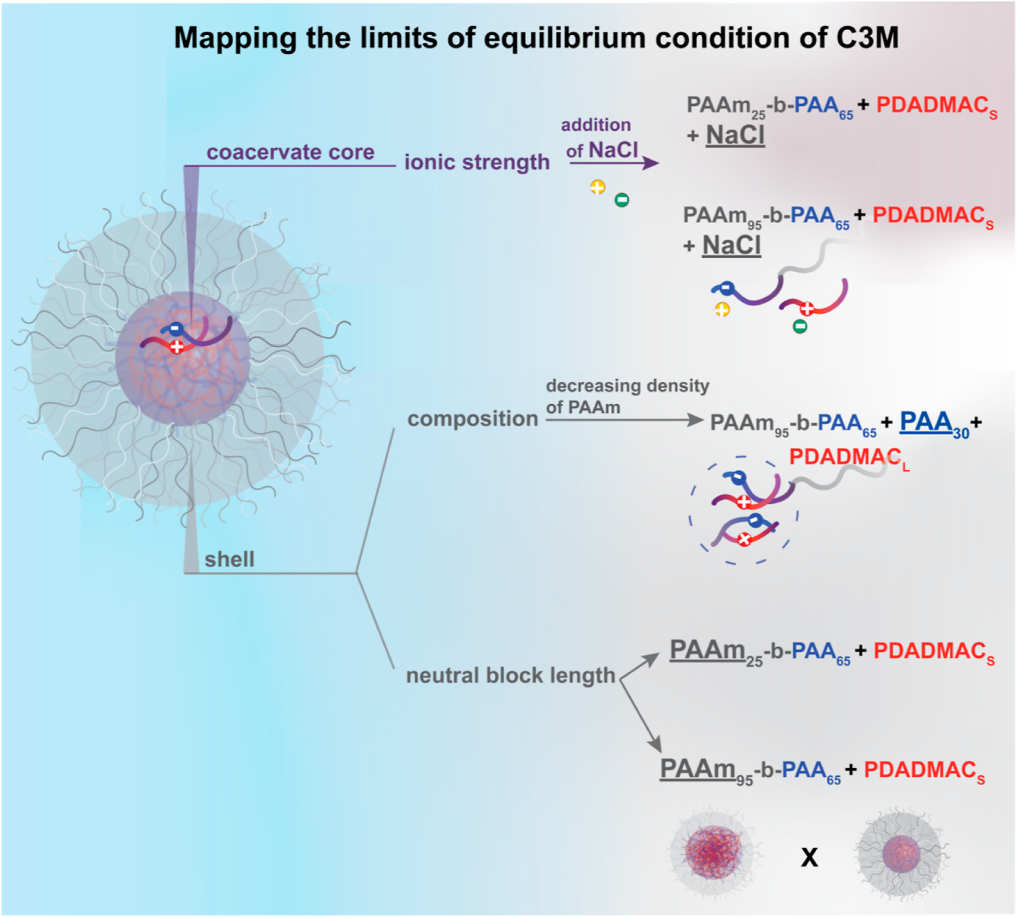

Figure 1. Schematic representation of the strategy used to map the limits of equilibrium conditions of C3Ms by varying the core (simple salt addition) and the shell (composition/density and neutral block length). Overview of the distinct polymers employed in each part of this work: negatively charged block and neutral block are shown in blue and gray, respectively, and positively charged homopolymer is shown in red.

One can use several procedures to obtain structural information from the scattering intensity. A powerful approach is the indirect Fourier transformation (IFT), which provides the so-called pair distance distribution function, $p(r)$, as defined in eq 3

$$p(r) = \frac{r^2}{2\pi^2}\int_0^\infty q^2 I_1(q)\frac{\sin(qr)}{qr}\mathrm{d}q \tag{3}$$

this method, initially introduced by Glatter,[34] was used in this work in a slightly different implementation.[35] D_{max} will be defined as the r-value, where the function $p(r)$ goes to zero.

For systems containing higher ionic strength, the presence of aggregates was noted, and therefore, a structure factor was considered. The combination of the IFT method with structure factor contributions (usually called the Generalized IFT method) allowed the decoupling of the single particle contribution ($p(r)$-function) and the system structure factor. This was done by the procedure described by Oliveira and co-workers.[35] As shown later in this article, the aggregate contributions could be well described by the use of the structure factor of globular aggregates with a given radius of gyration (R_G). The structure factor $S_{Gui}(q)$ is defined as

$$S_{Gui}(q) = 1 + Sc_{Gui}\exp\left(-\frac{q^2 R_G^2}{3}\right) \tag{4}$$

where Sc_{Gui} is the scale factor of the aggregate contribution and R_G is the average aggregate radius of gyration.

To go one step further on the system description, a model assuming a graded sphere for the coacervate was also used (this model is described in the Supporting Information). This model was based on the work of Fehér et al.[36] A spherically symmetric particle is assumed with a graded interface to the solvent.

RESULTS AND DISCUSSION

In this work, we investigated the stability of C3Ms formed by the charged-neutral diblock copolymer, PAAm-*b*-PAA, and an oppositely charged homopolymer, PDADMAC. In order to map the equilibrium boundaries, experiments were conducted to explore variations in both the aggregate core (by increasing the ionic strength and screening the polyelectrolyte charge) and the shell (by varying the neutral block length and shell composition). By systematically analyzing these factors, we sought to identify the specific limits within which C3Ms remain thermodynamically stable, providing valuable insights into their behavior and properties. Figure 1 schematically represents the strategy used to map the limits of the equilibrium condition of C3Ms, as well as rendering an overview of the different polymers employed in each part of our work.

Characterization of C3Ms at 1:1 Stoichiometry. We prepared C3Ms free of their small counterions with a 1:1

https://doi.org/10.1021/acs.langmuir.3c01606
Langmuir 2024, 40, 2015−2027

charge stoichiometry by using combinations of PDADMAC and $PAAm_x$-*b*-PAA_y of two different molecular weights. Concerning the copolymer, for all complexes prepared, the PAA block was kept constant, and neutral (PAAm) blocks of different molecular weights were used. Therefore, the effect of the C3Ms' shell on the structure and stability could be more directly assessed. These copolymers were combined with PDADMAC with two different molecular weights, and the corresponding hydrodynamic radii and zeta potential values of the resulting aggregates are listed in Table 2.

Table 2. Apparent Average Hydrodynamic Radius (R_H), PDI, and Zeta Potential (ζ) Values of C3Ms Free of Small Ions prepared by an Acid−Base Titration Methodology

complex salt C3M	R_H (nm)[a]	PDI[a]	ζ (mV)
$PAAm_{25}$-*b*-($PA_{65}PDADMA_S$)	44	0.04	−10
$PAAm_{25}$-*b*-($PA_{65}PDADMA_L$)	47	0.02	−4
$PAAm_{95}$-*b*-($PA_{65}PDADMA_S$)	41	0.06	−10
$PAAm_{95}$-*b*-($PA_{65}PDADMA_L$)	39	0.06	−8

[a]R_H and PDI values refer to DLS data measured using a detection angle of 90°.

According to the zeta potential values shown in Table 2, all aggregates prepared are close to charge neutrality, which is an indication that most polyelectrolytes remain assembled within the micellar core. The values of the hydrodynamic radii of the aggregates formed by copolymers with PAAm with two different molecular weights (Table 2) are all around 40−50 nm with no clear trend of variation, despite the differences in the polyelectrolyte molecules used. This general result agrees with findings reported by van der Burgh *et al.*[18] on similar C3Ms, who explained the constancy of the hydrodynamic radii, R_H, as a result of changes in their aggregation numbers. The authors assume that the R_H can be described by

$$R_H = H_{shell} + R_{core} \quad (5)$$

being R_{core} and H_{shell}, the radius of the core and the shell thickness of the aggregate, respectively. The aggregation number is sensitive to the length of the shell block because only a limited fraction of neutral chains can be positioned at the core−shell interface. Therefore, for a core block with constant size, it is expected that an increase in the shell block should result in a decrease in the aggregation number due to steric interaction between these neutral chains at the core−shell interface. In other words, the observed constancy in R_H values is a result of the compensation between the decrease in the core size and the increase in the shell thickness as the shell block increases.

The results presented in Table 2 also allow for the assessment of the effects of the homopolymer length. We found that changing the size of the homopolymer does not cause a significant change in the size of the C3Ms. A similar dependence between homopolymer size and C3M hydrodynamic radius was described by van der Kooij *et al.*[22] Those authors observed the existence of a critical homopolymer length for each diblock copolymer considered. For homopolymers smaller than this specific critical length, the hydrodynamic radius of C3M is approximately constant, and it should increase sharply beyond this value. Recently, Marras *et al.*[37] have proposed a scaling relationship between the hydrodynamic radius of C3Ms and these polymers' lengths. According to those authors, the C3M size increases strongly with the chain length of the charged block but decreases weakly or is independent of the chain length of the neutral block and the homopolyelectrolyte. Similarly, the authors also showed that the core radius also decreases slightly with the neutral block length as a result of the decrease in the number of aggregation. Overall, our findings agree with these previous reports.

To investigate the stability of the C3Ms, their size was monitored for 350 days using DLS measurements. The experiments were carried out in duplicate and, along this period, only negligible variations of the hydrodynamic radii and scattering intensity of the C3M solutions, as well as in their polydispersity values, were observed (see Figure S1). No indication of aggregation was observed, even for complex aggregates prepared with the copolymer containing the shortest neutral block. Therefore, considering the long period of observation and the previous picture that these are dynamic

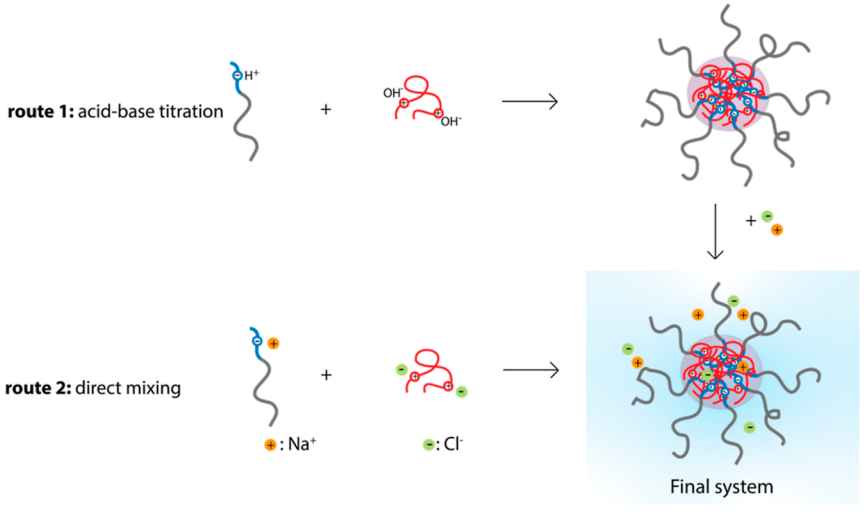

Figure 2. Schematic representation of the different C3M preparation routes: acid−base titration (route 1) and direct mixing (route 2). Both preparation protocols end at the same final composition (bottom right): same polymer concentration, pH 7.5, and [NaCl] = 1 mmol L^{-1}. Negatively charged block and neutral block are shown in blue and gray, respectively. Positively charged homopolymer is shown in red.

https://doi.org/10.1021/acs.langmuir.3c01606
Langmuir 2024, 40, 2015−2027

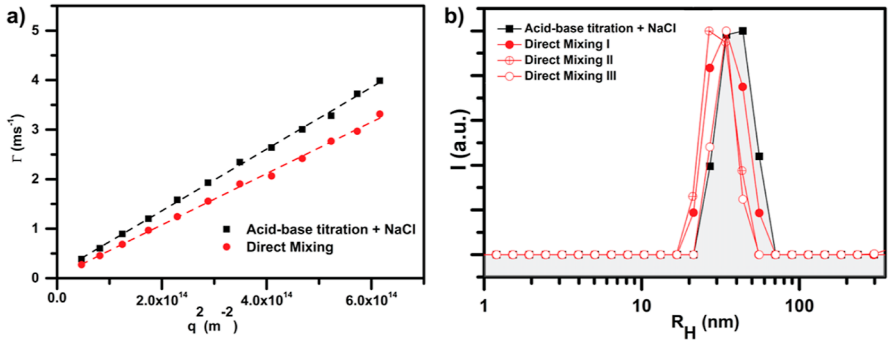

Figure 3. DLS results for aqueous mixtures of C3M ($PAAm_{95}$-*b*-PAA_{65} and $PDADMAC_S$) prepared by acid−base titration followed by the addition of NaCl (black) and direct mixing (red). The data refers to systems containing 0.015 wt % polymer, pH 7.5, and [NaCl] = 1 mmol L^{-1}. (a) Graphs of the decay rate $\Gamma(q)$ as a function of q^2. The dashed lines indicate the linear regression. The measurement was carried out in duplicate, and the error bars are smaller than the symbols. (b) Hydrodynamic radii (R_H) distribution of C3M prepared by two different procedures measured at the angle of 90°. Size distribution curves of C3M, which were independently prepared in triplicate by the direct mixing procedure (red).

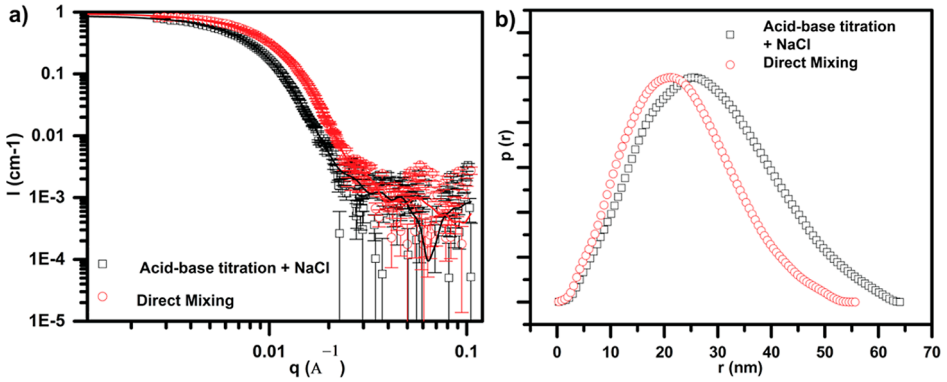

Figure 4. SAXS results for C3Ms ($PAAm_{95}$-*b*-PAA_{65} and $PDADMAC_S$) prepared by using two different routes: acid−base titration followed by the addition of NaCl and direct mixing. (a) Intensity curves in the absolute scale. The symbols and the continuous line represent the experimental data and the IFT fit, respectively. (b) Pair distance distribution function.

aggregates, these results corroborate the hypothesis that these C3Ms are thermodynamically stable species.

Consequently, if these aggregates are in thermodynamic equilibrium, their final structure should be independent of their preparation protocol, this being a good methodology to test this hypothesis.[19] Hence, C3Ms were prepared by using two different routes: direct mixing of the polyelectrolyte solutions and acid−base titration methodology followed by adjustment of the salt concentration. In the first one, direct mixing protocol, oppositely charged polymer solutions are mixed, both containing their counterions, until the 1:1 charge stoichiometry. On the other hand, in the acid−base titration procedure, the acid copolymer solution was added into the base homopolymer system up to the equivalence point. Next, a predetermined quantity of NaCl was added to adjust the ionic strength of the solution as in the direct mixing protocol. Therefore, both systems are at exactly the same composition and pH. This test was carried out by preparing C3M obtained from the combination of $PAAm_{95}$-*b*-PAA_{65} and $PDADMAC_S$. These different preparation routes are listed in Figure 2.

Indeed, by following such procedures, the final state of the C3Ms would be the same if they are in thermodynamic equilibrium, provided that no kinetic trapping occurs. Generally, the complexation between oppositely charged polyelectrolytes is due to electrostatic interaction, which is driven by an entropic effect resulting from the release of counterions[38] and water molecules.[3] In the acid−base titration method, the formation of the complex is driven by the electrostatic interaction that takes place after neutralization of the acid copolymer, $PAAm_{95}$-*b*-PAA_{65}, with the base homopolymer, $PDADMAOH_S$. The comparison between the nanoparticles prepared via these different routes was based on their hydrodynamic radii and the zeta potential values. For this evaluation, plots of the decay rates, $\Gamma(q)$, versus q^2 of the complexes prepared by the two different routes were measured in duplicate and are shown in Figure 3a. The diffusive nature of relaxation is confirmed by the linear dependence of the plots, allowing the determination of the aggregate's apparent diffusion coefficient, D_0, and the hydrodynamic radius, R_H. For polyelectrolyte complexes prepared using the acid−base titration methodology and the direct mixing procedure, the hydrodynamic radii were 39.7 ± 0.6 (PDI = 0.05) and 33.7 ± 0.8 nm (PDI = 0.05), respectively.

From the results of Figure 3, it is possible to observe that the values of the hydrodynamic radii of the C3M are very similar for the two protocols, especially considering the reproducibility deviation of the size distribution curves of C3Ms prepared by direct mixing (Figure 3b). Considering their distribution curves, the direct mixing methodology yields aggregates with a broader size distribution, which can be attributed to the inherent reproducibility of the preparation methodology. In this sense, the size distribution curves have a substantial overlap: the direct-mixing C3Ms exhibit radii starting from a minimum radius of 18 nm, whereas the acid−base-titration C3Ms display radii starting from 20 nm, with both reaching a size of 70 nm. Overall, the sizes measured by DLS for both

https://doi.org/10.1021/acs.langmuir.3c01606
Langmuir 2024, 40, 2015−2027

aggregates, also taking into account the 5% variation suggested by the PDI, are similar for both routes.

Moreover, based on the zeta potential values measured for C3Ms prepared by direct mixing and acid−base titration, respectively, −8 ± 1 and −7 ± 1 mV, we confirm that particles formed by both routes are essentially the same and close to the condition of charge neutrality. Thus, according to these results and considering the polydispersity and preparation reproducibility, we can conclude that both routes lead to the same final state. To further investigate the aggregates prepared by these different methodologies, we also performed small-angle X-ray scattering measurements (results shown in Figure 4) to evaluate their size and shape. The analysis of SAXS data from different routes was performed by the indirect Fourier transformation (IFT) method. The IFT method produces a model-free representation of the scattering data: the pair distance distribution function.

The scattering curves of both systems are slightly different, especially at $q > 0.01$ Å^{-1}. The micelles prepared by the direct mixing procedure display a slightly higher scattering intensity at a lower q region compared to those of acid−base titration followed by NaCl addition. The experimental data of SAXS from both systems were well-fitted using the IFT method, and their respective $p(r)$ functions were obtained. The $p(r)$ goes to zero at $r = D_{max}$, where D_{max} is the maximum distance within scattering objects. Remarkably, the aggregate prepared by direct mixing showed a relatively lower D_{max}. From the IFT method, it is also possible to obtain the particle radius of gyration, which is an indication of the root-mean-square radius of the particle. The R_G values for micelles prepared by the direct mixing and titration protocols are 18 ± 0.1 and 22 ± 0.2 nm, respectively, again, very close.

Additionally, the SAXS results were also fitted using an advanced model assuming a graded sphere with polymer contributions, as shown in detail in the Supporting Information. This model could successfully describe the SAXS data for both systems. The C3M radius obtained by both fitting methods is summarized in Table 3.

The agreement between both fitting methods confirms the good quality of the fits. Also, if we consider the effective radius obtained from the IFT method ($R_{eff} = \sqrt{5/3}R_G^{sph}$), it is systematically larger than the micelle radius obtained from the graded sphere method. The small difference in radius for the IFT and graded sphere models comes from the definition of the micelle radius made on the latter model. Since the outer radius of the sphere is diffuse, there is not a clear cutoff for the radius. This point is discussed in the Supporting Information. In summary, comparing the obtained parameters for each method, these results suggest that the shape and size of the cores, aggregation number, Nagg (shown in the Supporting Information), and size are very similar for C3Ms prepared by both routes, especially considering the intrinsic size variation of this type of aggregate.

Table 3. Obtained Radii from SAXS Analysis Include the Radius of Gyration (R_G), Effective Radius of a Sphere (R_{eff}), and Micelle Radius (R_{mic}) for C3Ms ($PAAm_{95}$-*b*-PAA_{65} and $PDADMAC_S$)[a]

method	parameters	direct mixing	acid−base titration
IFT	R_G [nm]	17.88 ± 0.1	21.85 ± 0.2
	R_{eff} [nm][b]	23.08 ± 0.1	28.21 ± 0.3
graded sphere[c]	R_{mic} [nm]	21.8 ± 0.2	26.4 ± 0.2

[a]These radii were determined by using various fitting methods. Specifically, the IFT method was utilized to calculate R_G and R_{eff}, while R_{mic} was determined using the graded sphere model (see SAXS analysis in the Supporting Information). [b]Calculated using the expression for a radius of gyration for a solid sphere, $R_G^{sph} = \sqrt{3/5}R_{eff}$. [c]For this model fit, the inner part of the micelle was fixed to 10 Å, the arm radius of gyration was fixed to 20 Å, and the number of arms used was 6. The values for the arm radius of gyration and the number of the arms of the star are typical for this type of system.

Effect of Shell Composition. In the previous section, the stability of C3Ms with different hydrophilic block lengths was investigated. Another way to verify the effect of the shell layer on the stability of the C3Ms is by replacing a fraction of the copolymer with the corresponding charged homopolymer in the complex, as presented in the scheme of Figure 1. This procedure would keep the charge neutrality in the core while decreasing the fraction of acrylamide blocks in the system. For this, the resulting aggregates contain three different components: $PAAm_{95}$-*b*-PAA_{65}, PAA_{30}, and $PDADMAC_L$, maintaining the charge ratio as 1:1.

Hofs et al.[39] proposed modifications in eq 5 to consider the hydrodynamic radius of the aggregate formed by other compositions, creating a compositional parameter, β. Thus, size could be related to system composition, shell thickness (H_{shell}), and the core radius with no added additional homopolyelectrolytes (R^0_{core}) by the following

$$R_H = H_{shell} + R^0_{core}\left(1 + \frac{N^-_{HP}}{N^-_{DB}}\right) = H_{shell} + R^0_{core}\beta \quad (6)$$

where N^-_{HP} is the total number of anionic monomers in the homopolyelectrolyte, N^-_{DB} is the number of anionic monomers in the charged block of the copolymer in the system, and the compositional parameter, β, is expressed as $1 + \frac{N^-_{HP}}{N^-_{DB}}$. This model was applied to the complexes formed by $PAAm_{95}$-*b*-PAA_{65}, PAA_{30}, and $PDADMAC_L$, and the behavior of the aggregate with different β was accessed by combining SAXS (Figure 5) and DLS as depicted in Figure 6. Considering the model, the different ratios of the number of monomers of the block copolymer and homopolymer, which are 0:100, 50:50, and 23:77, can be represented as $\beta = 1$, $\beta = 2$, and $\beta = 4.3$, respectively.

The changes in the hydrodynamic radius with β are shown to be linear, as presented in the black dotted line in Figure 6, which confirms that the model proposed by Hofs and coworkers[39] fits quite well the data for these complex sizes. It is clear that R_H is directly related to the composition of the system: the greater the degree of copolymer substitution, the larger the particle. In addition, the scattering intensity also increases with the β value. This agrees with the observations of those authors, who propose that despite the decrease in the number of aggregates (N) with β, there is an increase in their size and mass, and as $I \propto NR^6$, the scattering intensity also increases (Rayleigh scattering).[39] The independence of the particle radius from the detection angle indicates the formation of spherical aggregates.

The linear trend verified in the black dotted line in Figure 6 suggests that there was no change in the shape of the aggregates even for more extreme β values. To confirm the

https://doi.org/10.1021/acs.langmuir.3c01606
Langmuir 2024, 40, 2015−2027

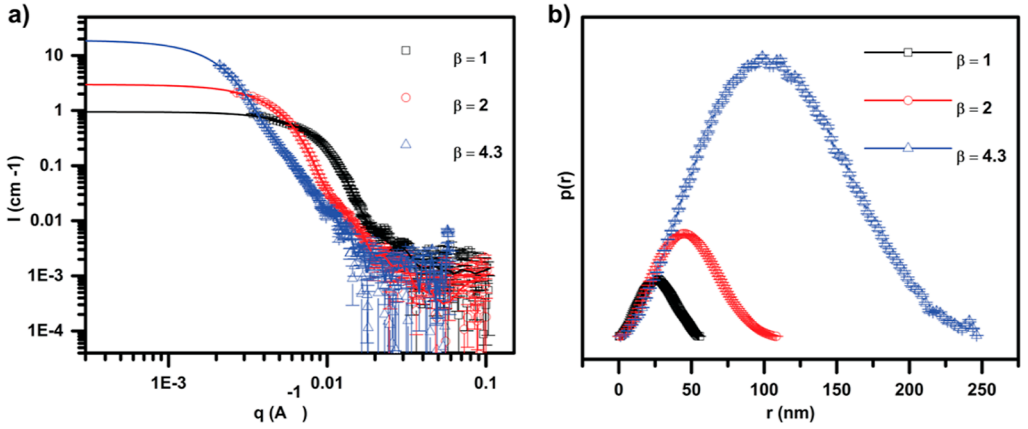

Figure 5. SAXS results for aggregates containing different compositional parameters ($\beta = 1 + \frac{N^{-}_{HP}}{N^{-}_{DB}}$): $\beta = 1$ (black), $\beta = 2$ (red), and $\beta = 4.3$ (blue). (a) Intensity curves in the absolute scale. The symbols and the continuous line represent the experimental data and the IFT fit, respectively. (b) Pair distance distribution function for aqueous mixtures of complexes.

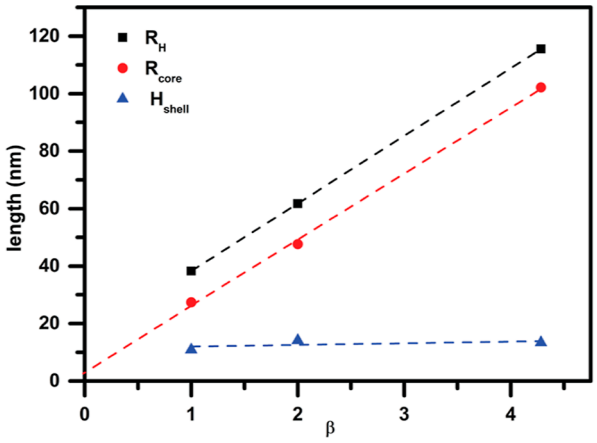

Figure 6. Length in the y-axis represents the dimensions of different parts of the C3M structure when varying the ratio (β) between PAA_{30} and $PAAm_{95}$-*b*-PAA_{65}: hydrodynamic radius (R_H, black square), core radius (R_{core}, red circle), and shell thickness (H_{shell}, blue triangle) of the aggregates. The dotted lines represent the linear regression for each of the C3M dimensions. These values were obtained by combining DLS and SAXS data (see text).

morphological behavior of the aggregates with different β values, SAXS measurements were performed (Figure 5).

The scattering curves of the different systems presented in Figure 5 are notably different. The micelles with larger β values display a higher scattering intensity compared to those with smaller β. Comparing the $p(r)$ functions of the systems, we can clearly verify that despite having different D_{max}, their curves display similar shapes. The $p(r)$ maximum is approximately at the center of the curves, and all of them display bell shapes. The shape of the curve of the $p(r)$ function provides an indication of the form of the scattering objects, suggesting that these aggregates are spherical. Therefore, SAXS data also provide evidence that, even decreasing the copolymer content in the system (but compensating it with the same charge homopolymer), the aggregates remain spherical.

From the DLS measurements, the hydrodynamic radius of the entire aggregate is determined. From the IFT analyses of the SAXS data, one mostly describes the relatively densely packed core that displays a much greater contrast compared with the highly hydrated outer shell. Consequently, SAXS data can be fitted to determine the core radius of C3M micelles.[37] Taken together, the shell thickness can be estimated by considering eq 5 ($H_{shell} = R_H - R_{core}$). Figure 6 summarizes the approximate values of the hydrodynamic radius (R_H), core radius (R_{core}), and shell thickness (H_{shell}) that were obtained for the aggregates in the range of the β value investigated.

As shown in Figure 6, the core and the hydrodynamic radius increase with β, while the shell thickness remains approximately constant over the range of β values investigated. Overall, this result suggests that an extra amount of complex coacervate is placed inside the entire aggregate, leading to its growth, while the shell content remains constant, including its thickness. Two different coacervate complexes may be present in the entire aggregate structure: one formed between the charged block of the copolymer with an oppositely charged homopolymer [$PAAm_{95}$-*b*-($PA_{65}PDADMA_L$)] and the other between both oppositely charged homopolymers ($PA_{30}PDADMA_L$). Therefore, considering the tendency of polyacrylamide to remain in the aqueous phase, the copolymer−homopolymer complex should be located preferentially at the interface of those large aggregates, with the inner core becoming richer in the other complex.

Interestingly, the model of Hofs et al.[39] (eq 6) also allows the determination of the values for H_{shell} and R^0_{core} of the C3M obtained through the linear fitting, in which the linear and angular coefficients are, respectively, H_{shell} = 15 nm and R^0_{core} = 23 nm. It is noteworthy that the core radius obtained from the SAXS results (R_{core} = 27 nm) agrees well with the value estimated by this model. The core radii can also be compared with the contour length of the PAA block. Possibly, the PAA blocks in the C3M core must be in a stretched conformation because the core radii are on the same order of magnitude as the contour lengths of PAA blocks (ca. 18 nm). A similar result was reported by Burgh and co-workers.[18] Following the same argument, the conformation of the PAAm at the surface of the C3M can also be considered by comparison with the contour length for $PAAm_{95}$, which is expected to be 26 nm (obtained from $L_c = 0.26N_{PAAm}$).[22] H_{shell} can also be compared with the value of 3 nm reported as the hydrodynamic radius of $PAAm_{140}$ in 1% wt. Overall, this comparison suggests that in these C3Ms, PAAm blocks are on average shorter but closer to an extended conformation than their random coils observed for homopolymers.

https://doi.org/10.1021/acs.langmuir.3c01606
Langmuir 2024, 40, 2015−2027

Interestingly, the use of the graded sphere model to adjust these data sets provides additional structural information. If single-graded spheres are assumed, good fits for the $\beta = 1$ data set can be obtained. However, that is not true for systems with $\beta = 2$ or $\beta = 4.3$. For these two cases, it was necessary to assume that the scattering particle is composed of aggregates of micelles, which were described by the Guinier structure factor. The fitting results are shown in Figure S6 and the resulting structural parameters, in Table S2.

Furthermore, since it was not possible to adjust the scattering curves as a simple and large micelle, these large aggregates cannot be organized as the simple core−shell model such as the micro-C3Ms proposed by Hofs et al.[39] However if we carefully analyze the fitting model used, instead of an increase in the size just of the core (micro-C3M model), those large aggregates are, in fact, homopolymer−homopolymer coacervates whose interface is surrounded by C3Ms. The result is a cluster with a raspberry-like structure where the large and globular aggregate is made of a core of homopolymer coacervate, which is stabilized in solution by C3Ms placed on its interface. This configuration may result as more favorable due to the increased interaction of homopolymer coacervates resulting from the relatively small amount of acrylamide blocks. The number of micelles in each aggregate is shown in Table S2 and, for instance, for samples with $\beta = 2$ and $\beta = 4.3$, each aggregate contains approximately 20 micelles.

Moreover, if the C3M core with $\beta = 1$ is spherical and displays the same density, assuming that it contains the same water content as a bulk coacervate (consisting of the homopolymers PAA_{30} and PDADMAC), then the core mass, m_c, of the aggregate with radius (r_{core}) can be estimated. The mass of the polyelectrolytes, m_p, in the core was obtained by subtracting the mass of water, m_w, from that of m_c ($m_p = m_c - m_w$). Following this procedure, the aggregation number of 1000 copolymer molecules per micelle was estimated (more details of the calculation are provided in Section S4 of the Supporting Information). As a comparison, the aggregation number estimated from the SAXS analyses discussed below has the same order of magnitude of polymer per micelle, estimated by using the bulk coacervate density approximation (see Supporting Information, topic S4 and S5).

Finally, when the copolymer is replaced by PAA, beyond a certain substitution degree, the C3Ms become unstable. This was investigated by measuring the hydrodynamic radii of these aggregates as a function of time at different proportions, represented by different β values. There was no change in the hydrodynamic size or in the polydispersity of the aggregates up to $\beta = 2$ during the analyzed period of 350 days, as can be observed in Figure S2. On the other hand, for systems with $\beta = 4.3$, changes in the hydrodynamic radius and formation of a macroscopic phase appear after 15 days. In these cases, it seems that the quantity of neutral blocks in the shell is no longer enough to ensure their stability and prevent phase separation.

Effect of Ionic Strength. In the previous sections, the frontiers of the equilibrium condition of C3M depending on the shell characteristics were investigated. Now, taking into account the core part of C3Ms as presented in the scheme of Figure 1, since its predominant interaction is Coulombic, the stability of the aggregate is expected to be influenced by the ionic strength of the surrounding medium. As the ionic strength increases, the polyelectrolyte charges become screened, and, at higher salt concentrations, the density of physical cross-links among the polyelectrolytes is reduced to a critical number, leading the aggregate to a complete dissociation.[22] In this sense, to elucidate the stability boundaries of C3M when the core structure is varied, C3M solutions in different ionic strength media were investigated. The C3M assemblies were previously formed, and then, NaCl was added from 1 to 300 mmol L^{-1}. The hydrodynamic radii of the particles were measured, and the results are shown in Figure 7.

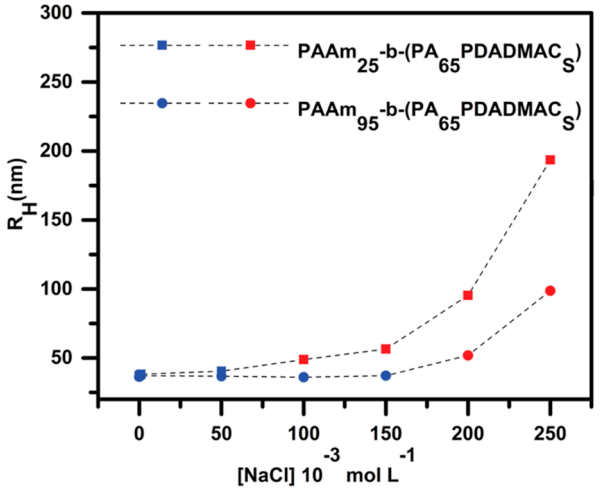

Figure 7. Hydrodynamic radius (R_H) of different complex salts, $PAAm_{25}$-*b*-(PA_{65}PDADMA$_S$) (squares) and $PAAm_{95}$-*b*-(PA_{65}PDADMA$_S$) (circles), as a function of NaCl concentration. Blue dots represent micelles in equilibrium, while the red ones denote unstable aggregates whose size varies over time. The error bars are smaller than the dots. All of the measurements were carried out right after complex preparation.

The curves in Figure 7 show two stages represented by the blue and red dots. In the regime of low salt concentrations, there is no significant variation in R_H (blue symbols). Beyond 100 mmol L^{-1} NaCl, R_H starts to increase considerably over time (red symbols). This variation is even more noticeable in the case of C3M containing the smallest PAAm block, whose size starts to increase at a lower NaCl concentration. Thus, for each complex, depending on the neutral block length, the limit between those two regions is different. The scattering intensity detected for all systems containing 300 mmol L^{-1} of NaCl is very low, this being interpreted as a sign of complete dissociation of the aggregate (Figure S3).

This general behavior is already known, with the breakdown of polymer ion pairs that are replaced by pairs between the simple ions and the polyelectrolytes (sometimes named extrinsic pairs), leading to the swelling of the C3Ms and, beyond a certain limit, their complete dissociation.[28] Questions remain as to whether this increase in size is due exclusively to the swelling of the complex, associated only with the increased hydration of the core.[39] Due to the swelling of the core, a decrease in the contrast of the refractive index, n, between the aggregate and water would be expected and, consequently, a decrease in the light scattering intensity [$I_s \propto (n_{C3M} - n_{H_2O})^2$]. However, Figure S3 shows the opposite behavior. As the ionic strength is enhanced, there is an increase in the size of those structures, and the scattering intensity for each aggregate also increases up to a certain limit (until 250 mmol L^{-1} of NaCl).

https://doi.org/10.1021/acs.langmuir.3c01606
Langmuir 2024, 40, 2015−2027

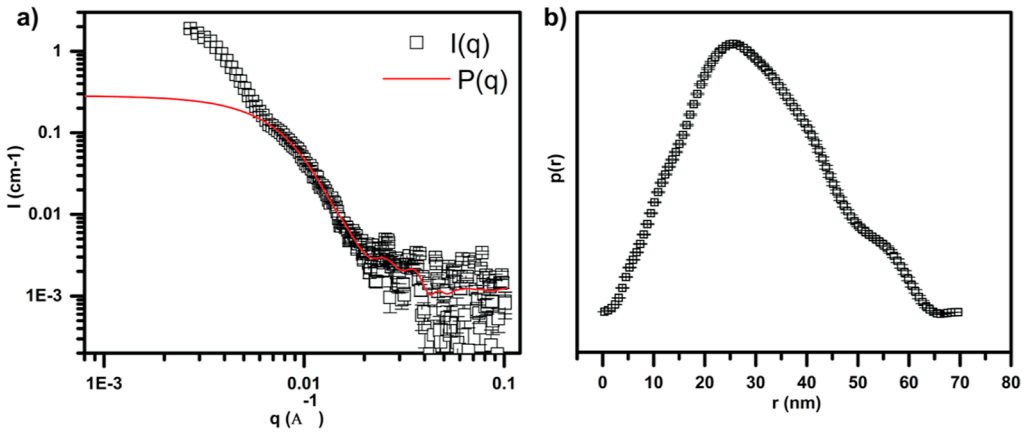

Figure 8. SAXS results for $PAAm_{95}$-*b*-($PA_{65}PDADMA_S$) in a system containing 200 mmol L^{-1} NaCl. (a) Intensity curves on the absolute scale. The symbols and the continuous line represent the experimental data and the IFT fit considering just the form factor [$P(q)$], respectively. (b) Pair distance distribution functions for aqueous mixtures of complexes. The measurement was carried out right after complex preparation.

This may be explained by the dominant dependency of I_s with R_H ($I_s \propto R_H^6$).

Furthermore, swelling of the core results in a change in the curvature of the aggregate to best accommodate its core with increasing volumes. This behavior can be explained by the concept associated with the critical packing parameter (p).[22] This is traditionally used for aggregates formed by amphiphilic molecules, and it can be calculated as $p = v_0/(al_0)$, l_0 and v_0 being the length and the volume of the hydrophobic tail, and a, the area occupied by the hydrophilic moiety at the surface of the aggregate. In analogy, the model applied to C3Ms considers that the polyelectrolyte complex corresponds to the hydrophobic portion as they are not miscible with water and the neutral block corresponds to the hydrophilic part. Therefore, at low salt concentrations, the curvature is high, and the C3Ms are preferentially spherical. However, for higher salt concentrations, the charge screening causes the swelling of the complex, leading to an increase in the core volume (v_0). Consequently, the aggregate curvature should decrease, favoring changes in its preferential morphology. Since the area occupied by the neutral block at the interface is smaller for shorter polyacrylamide blocks, this effect should be more prominent. Following this reasoning, the effects of salt on the size of the aggregate are expected to be more pronounced in the case of complexes containing a smaller neutral block, agreeing with the results shown in Figure 7.

Changes in the shape of the aggregate formed by $PAAm_{95}$-*b*-($PA_{65}PDADMA_s$) upon salt addition are expected, considering the length of the PAA chain. The maximum physically possible extension of this negative block, 18 nm, would not be enough to reach the center of these larger aggregates. In other words, if they remained spherical, their radii would be larger than the maximum length of PAA, which suggests that the resulting aggregates are no longer spherical. Similar behavior was also reported by van der Kooij et al.[22] for C3Ms formed by PAA_{13}/$PM2VP_{41}$-*b*-PEO_{204}, and they also proposed a morphological change in the shape of the aggregates: varying from spherical to elongated micelles.

To further confirm the shape of these large aggregates, SAXS measurements on the $PAAm_{95}$-*b*-($PA_{65}PDADMA_S$) system containing 200 mmol L^{-1} NaCl were also performed. For analysis of the curves of this system, the interaction between the aggregates had to be taken into account because its structure factor could not be neglected. The experimental data were fitted by decoupling the form factor from the structure factor. The form factor was adjusted based on the $p(r)$ function of the scattering particles, that is, the $p(r)$ function was obtained considering only the q range above 0.0067 $Å^{-1}$. The structure factor of this system was described by considering that large clusters are formed by the packing of C3M subunits. These clusters are represented by the Guinier structure factor $S_{Gui}(q)$, defined by eq 4, which assumes the formation of aggregates with a globular shape with the radius of gyration, R_G. The fitting result is given by the red and blue lines in Figure 8.

A notable change in the scattering intensity profile of the aggregate at a high ionic strength system can be verified in Figure 8. A shape difference in the $p(r)$ function of C3M with the addition of a high NaCl concentration is also noteworthy, and this confirms a morphological transition for this aggregate. The $p(r)$ maximum is shifted toward the lower D range of the curve, which no longer presents a bell shape. As mentioned in the previous sections, the tendency of the C3Ms to reach larger sizes in the $p(r)$ curve can be understood as an effect of the diffuse outer layer that composes the micelles. The IFT results were also compared to the ones obtained using the graded sphere model (Figure S7 and Table S3).

Interestingly, the D_{max} for a high ionic strength system does not increase greatly compared to that for C3M without salt. This result suggests that even with a morphological change of the C3M aggregates with the increase in the ionic strength, there is no great change in the size of the aggregates. This SAXS result could indicate a discrepancy in the hydrodynamic radius obtained by DLS (Figure 7). However, the structure factor that best fits the experimental data considers the fact that subunits of C3Ms are packed together, forming larger clusters. From the results shown in Table S3, considering the IFT method and the graded sphere model, the results indicate that ~15−20 micelles form the larger aggregate in the system containing 200 mmol L^{-1} of NaCl. This means that the increase in ionic strength not only results in the swelling and morphological change of the C3Ms but also leads to a loss of colloidal stability and consequent aggregation into larger clusters. Such larger objects are observed by light scattering and are characterized by their hydrodynamic radius.

Assessing Equilibrium Conditions. Considering the acid−base titration methodology,[27] C3Ms were prepared in the absence of their smaller counterions and at 1:1 charge

https://doi.org/10.1021/acs.langmuir.3c01606
Langmuir 2024, 40, 2015−2027

stoichiometry between the oppositely charged polyelectrolytes. Nanometric aggregates with similar sizes and close-to-charge neutrality conditions were obtained (Table 2). Similar aggregates were also obtained using a different pathway: a direct mixing protocol. The comparison between the resulting structures is fundamental to determining the nature of the stability of the C3Ms. Our results have shown that for C3Ms at the 1:1 stoichiometry, the observed hydrodynamic radii and morphology of the aggregates prepared by using the two paths are essentially the same, within the uncertainties of each preparation and measurement. This observed independence from the preparation protocol reinforces that these aggregates are in a thermodynamic equilibrium state.

In the present study, the possible limits of the C3M equilibrium regime were also investigated, as presented in Figure 1. The effect of the aggregate shell on the C3M stability was investigated by the partial replacement of the copolymer by the same charge homopolymer, maintaining the charge ratio at 1:1. Thus, the number of neutral blocks in the system was reduced with the increase in the substitution degree by homopolymers with the same charge. According to the results shown in Figure 6, the greater this substitution (β), the larger the size of the aggregate. Interestingly, SAXS measurements demonstrated that no morphological changes were observed for the entire aggregate within the range of β values investigated. Consequently, the relationship of β with the observed stability of the C3Ms could also be determined. For β values up to 2, during 350 days of observation, no changes in the hydrodynamic radius or the polydispersity of the aggregates were observed. However, for C3Ms prepared with β = 4.3, changes in the hydrodynamic radius were observed, and a macroscopic phase separation was also noticed around 15 days after the preparation of the system, indicating that this system crossed the equilibrium limit.

In addition to the stability, a great advantage of these systems is the possibility of predicting the size of these swollen C3Ms using the linear equation obtained considering the model described by Hofs and co-workers.[39] In this sense, the C3M core can be tuned by varying the ratio between the copolymer and the homopolymer. This result motivates the use of these tunable and stable structures, for instance, as platforms for the encapsulation of biomacromolecules, such as enzymes and nucleic acids, owing to the possibility of regulating their size depending on the desired application.

The limit between the thermodynamic and kinetic stability of C3Ms was also assessed by focusing on the C3M core and increasing the simple salt concentration, as shown in Figure 7. This affects directly the polyelectrolyte pairs in the core. Above a certain salt content, the hydrodynamic radius of C3M increases considerably. For C3Ms with a smaller block of polyacrylamide, $PAAm_{25}$-*b*-($PA_{65}PDADMA_S$), aggregate growth can be observed above 50 mmol L^{-1}. On the other hand, no size variation was verified for the C3Ms with a larger neutral block, $PAAm_{95}$-*b*-($PA_{65}PDADMA_S$), below a NaCl concentration of 100 mmol L^{-1}. This is a strong indication of the formation of stable aggregates. A metastable aggregate was just verified above this salt concentration, in which quasi-spherical C3Ms give way to anisotropic ones, and it aggregates into larger clusters (Figure 8), as confirmed by the analyses of the SAXS results.

Therefore, by combining different previous studies and based on the results presented here, we are able to define the conditions under which equilibrium C3Ms are expected. First of all, equilibrium micelles are formed preferentially at polyelectrolyte mixing ratios close to the 1:1 charge composition.[40] The length and the chemical nature of the shell block composition are also relevant to forming stable structures.[18] The nature of the polyelectrolyte ionic groups influences the core properties and the presence of additional interactions, due to which solid and frozen cores can also be formed.[41] In addition, no micelles are formed where there is a very asymmetric block length.[18] Finally, stable micelles are expected depending on the shell density (β values up to 2) and simple salt concentration below the NaCl concentration of 100 mmol L^{-1}.

CONCLUSIONS

In the present work, we analyzed C3Ms prepared with $PAAm_{95}$-*b*-PAA_{65} and PDADMA by two different protocols: direct mixing and acid−base titration, followed by salt addition. The structure of the resulting C3Ms was close in terms of the charge neutrality, size, and shape of the aggregates, as probed by DLS and SAXS measurements. The obtained structural parameters and the verification that their structures did not vary over long time periods suggest that these C3Ms are in an equilibrium condition.

Additionally, the boundaries between the thermodynamic and kinetic regimes of C3M stability were assessed toward the partial replacement of the copolymer and by changing the medium ionic strength. By decreasing the charged-neutral diblock copolymer content in the system (decreasing β), the complexes reach a metastable state, eventually resulting in phase separation. For $PAAm_{95}$-*b*-($PA_{65}PDADMA_S$), above the NaCl concentration of 100 mmol L^{-1}, the amount of salt was sufficient to affect the stability of the complex, so the effect of aging became noticeable, and a rapid increase in the hydrodynamic radius of the aggregates was observed. We emphasize that the effect of ionic strength is proven to be directly related to the size of the poly(acrylamide) block: the smaller the neutral block, the more evident the growth of the aggregate, with less salt being sufficient to promote the increase in R_H values.

Overall, these results confirm that under certain conditions, coacervate micelles, C3Ms, indeed form equilibrium aggregates, and they also indicate how these micelles respond to changes in their composition, polymer architecture, and medium conditions such as salt concentration. This body of evidence constitutes relevant information considering the potential application of these micelles for encapsulation,[13,42] drug delivery,[16] and other controlled release platforms.[17,43,44]

ASSOCIATED CONTENT

Supporting Information

The Supporting Information is available free of charge at https://pubs.acs.org/doi/10.1021/acs.langmuir.3c01606.

Additional experimental details about the aging effect of C3Ms and SAXS fitting model methods, including the calculation of the number of aggregates of C3Ms based on different methods (PDF)

AUTHOR INFORMATION

Corresponding Author

Watson Loh − *Institute of Chemistry, University of Campinas (UNICAMP), 13083-970 Campinas, São Paulo, Brazil;*

https://doi.org/10.1021/acs.langmuir.3c01606
Langmuir 2024, 40, 2015−2027

orcid.org/0000-0002-8049-3321; Email: wloh@unicamp.br

Authors

Júlia Bonesso Sabadini − *Institute of Chemistry, University of Campinas (UNICAMP), 13083-970 Campinas, São Paulo, Brazil;* orcid.org/0000-0002-5966-8609

Cristiano Luis Pinto Oliveira − *Institute of Physics, University of São Paulo (USP), 05508-090 São Paulo, São Paulo, Brazil;* orcid.org/0000-0002-3426-6507

Complete contact information is available at: https://pubs.acs.org/10.1021/acs.langmuir.3c01606

Notes

The authors declare no competing financial interest.

■ ACKNOWLEDGMENTS

The authors gratefully acknowledge the São Paulo Research Foundation FAPESP for financial support through projects 2015/25406-5 and 2021/12071-6 and for scholarships to J.B.S. (2018/25041-5, 2020/11735-5, and 2021/11317-1). W.L. also thanks the Brazilian Agency CNPq for a senior researcher grant (grant number 306398/2018-4).

■ REFERENCES

(1) Sing, C. E.; Perry, S. L. Recent Progress in the Science of Complex Coacervation. *Soft Matter* **2020**, *16* (12), 2885−2914.
(2) Fu, J.; Schlenoff, J. B. Driving Forces for Oppositely Charged Polyion Association in Aqueous Solutions: Enthalpic, Entropic, but Not Electrostatic. *J. Am. Chem. Soc.* **2016**, *138* (3), 980−990.
(3) Park, S.; Barnes, R.; Lin, Y.; Jeon, B.; Najafi, S.; Delaney, K. T.; Fredrickson, G. H.; Shea, J.-E.; Hwang, D. S.; Han, S. Dehydration Entropy Drives Liquid-Liquid Phase Separation by Molecular Crowding. *Commun. Chem.* **2020**, *3* (1), 83.
(4) Laugel, N.; Betscha, C.; Winterhalter, M.; Voegel, J.-C.; Schaaf, P.; Ball, V. Relationship between the Growth Regime of Polyelectrolyte Multilayers and the Polyanion/Polycation Complexation Enthalpy. *J. Phys. Chem. B* **2006**, *110* (39), 19443−19449.
(5) Gucht, J. v. d.; Spruijt, E.; Lemmers, M.; Cohen Stuart, M. A. Polyelectrolyte Complexes: Bulk Phases and Colloidal Systems. *J. Colloid Interface Sci.* **2011**, *361* (2), 407−422.
(6) Voets, I. K.; de Keizer, A.; Cohen Stuart, M. A. Complex Coacervate Core Micelles. *Adv. Colloid Interface Sci.* **2009**, *147*−*148*, 300−318.
(7) Lindhoud, S.; Norde, W.; Cohen Stuart, M. A. Effects of Polyelectrolyte Complex Micelles and Their Components on the Enzymatic Activity of Lipase. *Langmuir* **2010**, *26* (12), 9802−9808.
(8) Lindhoud, S.; de Vries, R.; Schweins, R.; Cohen Stuart, M. A.; Norde, W. Salt-Induced Release of Lipase from Polyelectrolyte Complex Micelles. *Soft Matter* **2009**, *5* (1), 242−250.
(9) Kawamura, A.; Yoshioka, Y.; Harada, A.; Kono, K. Acceleration of Enzymatic Reaction of Trypsin through the Formation of Water-Soluble Complexes with Poly(ethylene glycol)-*block*-Poly(α,β-aspartic acid). *Biomacromolecules* **2005**, *6* (2), 627−631.
(10) Sureka, H. V.; Obermeyer, A. C.; Flores, R. J.; Olsen, B. D. Catalytic Biosensors from Complex Coacervate Core Micelle (C3M) Thin Films. *ACS Appl. Mater. Interfaces* **2019**, *11* (35), 32354−32365.
(11) Lindhoud, S.; Norde, W.; Cohen Stuart, M. A. Reversibility and Relaxation Behavior of Polyelectrolyte Complex Micelle Formation. *J. Phys. Chem. B* **2009**, *113* (16), 5431−5439.
(12) Blocher McTigue, W. C.; Perry, S. L. Design Rules for Encapsulating Proteins into Complex Coacervates. *Soft Matter* **2019**, *15* (15), 3089−3103.
(13) Blocher McTigue, W. C.; Perry, S. L. Protein Encapsulation Using Complex Coacervates: What Nature Has to Teach Us. *Small* **2020**, *16* (27), 1907671.
(14) McClements, D. J. Encapsulation, Protection, and Delivery of Bioactive Proteins and Peptides Using Nanoparticle and Microparticle Systems: A Review. *Adv. Colloid Interface Sci.* **2018**, *253*, 1−22.
(15) Perry, S. L.; McClements, D. J. Recent Advances in Encapsulation, Protection, and Oral Delivery of Bioactive Proteins and Peptides Using Colloidal Systems. *Molecules* **2020**, *25*, 1161.
(16) Blocher, W. C.; Perry, S. L. Complex Coacervate-Based Materials for Biomedicine. *Wiley Interdiscip. Rev.: Nanomed. Nanobiotechnology* **2017**, *9* (4), No. e1442.
(17) Magana, J. R.; Sproncken, C. C. M.; Voets, I. K. On Complex Coacervate Core Micelles: Structure-Function Perspectives. *Polymers* **2020**, *12*, 1953.
(18) Van Der Burgh, S.; De Keizer, A.; Cohen Stuart, M. A. Complex Coacervation Core Micelles. Colloidal Stability and Aggregation Mechanism. *Langmuir* **2004**, *20* (4), 1073−1084.
(19) Wu, H.; Ting, J. M.; Werba, O.; Meng, S.; Tirrell, M. V. Non-Equilibrium Phenomena and Kinetic Pathways in Self-Assembled Polyelectrolyte Complexes. *J. Chem. Phys.* **2018**, *149* (16), 163330.
(20) Blocher McTigue, W. C.; Voke, E.; Chang, L.-W.; Perry, S. L. The Benefit of Poor Mixing: Kinetics of Coacervation. *Phys. Chem. Chem. Phys.* **2020**, *22* (36), 20643−20657.
(21) Vitorazi, L.; Ould-Moussa, N.; Sekar, S.; Fresnais, J.; Loh, W.; Chapel, J.-P.; Berret, J.-F. Evidence of a Two-Step Process and Pathway Dependency in the Thermodynamics of Poly(Diallyldimethylammonium Chloride)/Poly(Sodium Acrylate) Complexation. *Soft Matter* **2014**, *10* (47), 9496−9505.
(22) van der Kooij, H. M.; Spruijt, E.; Voets, I. K.; Fokkink, R.; Cohen Stuart, M. A.; van der Gucht, J. On the Stability and Morphology of Complex Coacervate Core Micelles: From Spherical to Wormlike Micelles. *Langmuir* **2012**, *28* (40), 14180−14191.
(23) Hofs, B.; de Keizer, A.; Cohen Stuart, M. A. On the Stability of (Highly Aggregated) Polyelectrolyte Complexes Containing a Charged-Block-Neutral Diblock Copolymer. *J. Phys. Chem. B* **2007**, *111* (20), 5621−5627.
(24) Holappa, S.; Kantonen, L.; Andersson, T.; Winnik, F.; Tenhu, H. Overcharging of Polyelectrolyte Complexes by the Guest Polyelectrolyte Studied by Fluorescence Spectroscopy. *Langmuir* **2005**, *21* (24), 11431−11438.
(25) Bakeev, K. N.; Izumrudov, V. A.; Kuchanov, S. I.; Zezin, A. B.; Kabanov, V. A. Kinetics and Mechanism of Interpolyelectrolyte Exchange and Addition Reactions. *Macromolecules* **1992**, *25* (17), 4249−4254.
(26) Kim, D.; Matsuoka, H.; Yusa, S.; Saruwatari, Y. Collapse Behavior of Polyion Complex (PIC) Micelles upon Salt Addition and Reforming Behavior by Dialysis and Its Temperature Responsivity. *Langmuir* **2020**, *36* (51), 15485−15492.
(27) Svensson, A.; Piculell, L.; Cabane, B.; Ilekti, P. A New Approach to the Phase Behavior of Oppositely Charged Polymers and Surfactants. *J. Phys. Chem. B* **2002**, *106* (5), 1013−1018.
(28) Queirós, M. V. A.; Loh, W. Preparation of Poly(Acrylate)/Poly(Diallyldimethylammonium) Coacervates without Small Counterions and Their Phase Behavior upon Salt Addition towards Poly-Ions Segregation. *Polymers* **2021**, *13* (14), 2259.
(29) Vitorazi, L.; Berret, J.-F.; Loh, W. Self-Assembly of Complex Salts of Cationic Surfactants and Anionic-Neutral Block Copolymers. Dispersions with Liquid-Crystalline Internal Structure. *Langmuir* **2013**, *29* (46), 14024−14033.
(30) Piculell, L.; Norrman, J.; Svensson, A. V.; Lynch, I.; Bernardes, J. S.; Loh, W. Ionic Surfactants with Polymeric Counterions. *Adv. Colloid Interface Sci.* **2009**, *147*−*148*, 228−236.
(31) Ferreira, G. A.; Piculell, L.; Loh, W. Hydration-Dependent Hierarchical Structures in Block Copolymer-Surfactant Complex Salts. *Macromolecules* **2018**, *51* (23), 9915−9924.
(32) Hammersley, A. P. FIT2D: A Multi-Purpose Data Reduction, Analysis and Visualization Program. *J. Appl. Crystallogr.* **2016**, *49*, 646−652.
(33) Pinto Oliveira, C. L. Investigating Macromolecular Complexes in Solution by Small Angle X-Ray Scattering. *Current Trends in X-ray Crystallography*; IntechOpen, 2011.

(34) Glatter, O. A New Method for the Evaluation of Small-Angle Scattering Data. *J. Appl. Crystallogr.* **1977**, *10* (5), 415−421.
(35) Oliveira, C. L. P.; Behrens, M. A.; Pedersen, J. S.; Erlacher, K.; Otzen, D.; Pedersen, J. S. A SAXS Study of Glucagon Fibrillation. *J. Mol. Biol.* **2009**, *387* (1), 147−161.
(36) Fehér, B.; Zhu, K.; Nyström, B.; Varga, I.; Pedersen, J. S. Effect of Temperature and Ionic Strength on Micellar Aggregates of Oppositely Charged Thermoresponsive Block Copolymer Polyelectrolytes. *Langmuir* **2019**, *35* (42), 13614−13623.
(37) Marras, A. E.; Campagna, T. R.; Vieregg, J. R.; Tirrell, M. V. Physical Property Scaling Relationships for Polyelectrolyte Complex Micelles. *Macromolecules* **2021**, *54* (13), 6585−6594.
(38) Yang, M.; Digby, Z. A.; Schlenoff, J. B. Precision Doping of Polyelectrolyte Complexes: Insight on the Role of Ions. *Macromolecules* **2020**, *53* (13), 5465−5474.
(39) Hofs, B.; de Keizer, A.; van der Burgh, S.; Leermakers, F. A. M.; Cohen Stuart, M. A.; Millard, P.-E.; Müller, A. H. E. Complex Coacervate Core Micro-Emulsions. *Soft Matter* **2008**, *4* (7), 1473−1482.
(40) Cohen Stuart, M. A.; Besseling, N. A. M.; Fokkink, R. G. Formation of Micelles with Complex Coacervate Cores. *Langmuir* **1998**, *14* (24), 6846−6849.
(41) Perry, S. L.; Leon, L.; Hoffmann, K. Q.; Kade, M. J.; Priftis, D.; Black, K. A.; Wong, D.; Klein, R. A.; Pierce, C. F.; Margossian, K. O.; Whitmer, J. K.; Qin, J.; de Pablo, J. J.; Tirrell, M. Chirality-Selected Phase Behaviour in Ionic Polypeptide Complexes. *Nat. Commun.* **2015**, *6* (1), 6052.
(42) Lueckheide, M.; Vieregg, J. R.; Bologna, A. J.; Leon, L.; Tirrell, M. V. Structure-Property Relationships of Oligonucleotide Polyelectrolyte Complex Micelles. *Nano Lett.* **2018**, *18* (11), 7111−7117.
(43) Otoni, C. G.; Queirós, M. V. A.; Sabadini, J. B.; Rojas, O. J.; Loh, W. Charge Matters: Electrostatic Complexation As a Green Approach to Assemble Advanced Functional Materials. *ACS Omega* **2020**, *5* (3), 1296−1304.
(44) Zhou, Z.; Yeh, C. F.; Mellas, M.; Oh, M. J.; Zhu, J.; Li, J.; Huang, R. T.; Harrison, D. L.; Shentu, T. P.; Wu, D.; Lueckheide, M.; Carver, L.; Chung, E. J.; Leon, L.; Yang, K. C.; Tirrell, M. V.; Fang, Y. Targeted Polyelectrolyte Complex Micelles Treat Vascular Complications in Vivo. *Proc. Natl. Acad. Sci. U.S.A.* **2021**, *118* (50), No. e2114842118.

https://doi.org/10.1021/acs.langmuir.3c01606
Langmuir 2024, 40, 2015−2027